Macromolecules
Article
pubs.acs.org/Macromolecules

Softwood Lignin-Based Methacrylate Polymers with Tunable Thermal and Viscoelastic Properties

Angela L. Holmberg,[†] Ngoc A. Nguyen,[‡] Michael G. Karavolias,[†] Kaleigh H. Reno,[†,§] Richard P. Wool,[†,§] and Thomas H. Epps, III*,[†,‡]

[†]Department of Chemical and Biomolecular Engineering, [‡]Department of Materials Science and Engineering, and [§]Center for Composite Materials, University of Delaware, Newark, Delaware 19716, United States

Supporting Information

ABSTRACT: Softwood (guaiacylic) lignin-based methacrylate polymers (LBMPs) that exhibit excellent glass transition temperatures (T_g's), desirable thermal stabilities (greater than 100 °C above T_g), and intermediate shear-flow resistances, in comparison to polystyrene and poly(methyl methacrylate), are reported herein. Different R-groups (*p*-position hydrogen, methyl, ethyl, and formyl groups) in otherwise homologous LBMPs impart distinct characteristics to the flow behavior and thermal properties of these bio-based polymers, which permit the investigation of unique structure−property relationships. More specifically, the zero-shear viscosities (η_0's) for the LBMPs span nearly 2 orders of magnitude as the R-group is varied, while the characteristic degradation temperatures differ more modestly (by ≈50 °C over the same series of polymers), and the T_g's exhibit minimal, yet application relevant, variations between ≈110 and ≈130 °C. These property differences were probed independent of tacticity, molecular weight, and dispersity effects due to the nature of the well-controlled macromolecules generated via reversible addition−fragmentation chain-transfer polymerization. Furthermore, heteropolymers prepared from mixtures of the lignin-based monomers have composition-dependent T_g's and component-dependent thermal degradation temperatures, thermolysis rates, and η_0's. The multicomponent materials demonstrate the enhanced tunability inherent in LBMPs. Altogether, this versatile library of softwood lignin-based monomers, and the unique structure−property relationships intrinsic to the resulting polymers, provides a unique platform for building potentially low-cost, high-performance, and bio-based viscoelastic materials attractive for thermoplastic elastomer and binder applications.

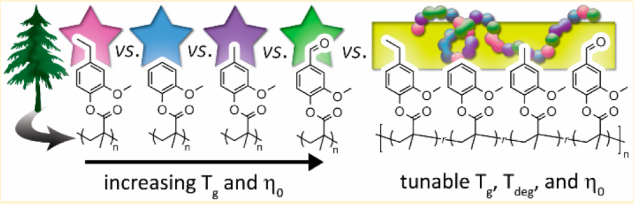

INTRODUCTION

Practical bio-based materials that can compete with petroleum-based plastics in both cost and performance are of growing interest yet are challenging to design due to trade-offs between cost, feedstock sustainability, and macromolecular properties.[1−3] An especially significant void exists for bio-based polymers with glass transition temperatures (T_g's) ≥ 100 °C.[1] Lignin has the potential to provide monomers that can fill this void, as it is an inexpensive, abundant, and renewable waste product with significant aromaticity.[1,4−9]

Several groups have taken chemicals found in (or prepared from) natural products or lignin-based bio-oils, such as β-methylstyrenes[10] or derivatives of butyrolactones,[11−13] glucose,[14] terpenes,[15−17] vanillin,[18] and isosorbide,[19] and employed controlled polymerization techniques to generate materials with T_g's ≥ 106 °C and other potentially desirable properties.[1,20] Controlled synthesis methods, such as reversible addition−fragmentation chain-transfer (RAFT) polymerization, unlock possibilities for these bio-based monomers to be incorporated into block polymers for applications such as thermoplastic elastomers, pressure-sensitive adhesives, and composite binders.[1] However, in these controlled syntheses of bio-based polymers, generally only one or two chemically distinct monomers are employed. Such homopolymers and copolymers may be expensive to produce, as separating complex bio-oils into single- or two-component streams would increase costs significantly.[1,2,21,22] A more effective means for delivering cost-effective bio-based polymers should involve capitalizing on the exceptional molecular diversity of bio-oils by building multicomponent polymers (heteropolymers) from mixtures of bio-oil components.[4,23−25] Polymerizing bio-oil components together could ameliorate separations costs while also providing a means to tailor polymer properties, such as T_g, thermal stability, and viscoelasticity, by adjusting bio-oil composition.

Softwood lignin-based bio-oils, such as those from pine or cedar trees, are ideal for these endeavors in multicomponent bio-based polymers as they largely consist of homologous aromatic compounds,[26−28] and the aromaticity of these molecules is expected to provide corresponding polymers with desirable T_g's, viscoelasticities, and mechanical strengths.[18,24,29,30] Components of softwood lignin bio-oils bearing a single hydroxyl functionality predominantly include 4-methoxyphenols, such as guaiacol, 4-ethylguaiacol, creosol, and

Received: October 22, 2015
Revised: January 16, 2016

vanillin.[26−28] For example, 78−83 wt % of the gas chromatography detectable components of crude Kraft lignin-based bio-oils (23−34 wt % of the total bio-oil) as reported by Choi et al. were 4-methoxyphenols (41−50 wt % guaiacol, 5−8 wt % 4-ethylguaiacol, 11−13 wt % creosol, 4−6 wt % vanillin, etc.).[28] These guaiacolic components can be acylated readily to methacrylate monomers[24,29] (2-methoxyphenyl methacrylate derivatives) that have similar reactivities, allowing for the straightforward synthesis of linear polymers with precise molecular weights, narrow dispersities, and approximately random distributions of monomer segments in each chain.[23] However, to make the most practical materials from such bio-oils, one needs to predict *a priori* the properties of multicomponent polymers based on the polymerization conditions and bio-oil composition.[23] This goal requires an understanding of the components' underlying structure−property relationships, some of which also may be applicable to explaining the varying properties of lignins themselves.[31]

The prediction of polymer properties from a structural basis is an immense challenge, especially for methacrylates, which have characteristics that depend significantly on tacticity and side-chain functionality.[32−34] For example, the T_g's for isotactic versus syndiotactic poly(methyl methacrylate) (PMMA) can differ by ≈70 °C,[33,35] and the T_g's for PMMA versus poly(ethyl methacrylate) can differ by ≈40 °C.[34] Quantitative structure−property relationships (QSPRs) for predicting polymer characteristics can be calibrated to sets of polymerized methacrylates to describe these significant differences between T_g that result from various polymer architectures, but model accuracy is limited by the amount and quality of available literature data.[32] Bertinetto et al.[32] compiled T_g and tacticity data from the literature for 110 phenyl-group-containing poly(meth)acrylic esters, but only two examples were derived from methoxy phenols (and those phenols had methoxy groups in the 3- and 4-positions instead of the 2-position as it is for guaiacol). Some seminal works compare the T_g's of poly(phenyl methacrylate)s and derivatives with single methyl, isobutyl, *tert*-butyl, methoxy, and other functionalities in various positions around the phenyl ring;[36,37] however, differences in molecular weights and variable tacticities make structure−property comparisons difficult. Thus, the relationships between side-chain aromatic groups carrying different functional groups and polymer properties, such as T_g, thermal stability, and viscoelasticity, need further investigation.

Herein, the thermal and viscoelastic properties of RAFT-synthesized softwood lignin-based methacrylate polymers (LBMPs, Scheme 1) are reported and compared to other common glassy polymers, viz., PMMA and polystyrene (PS). Two of the LBMPs are heteropolymers, in which one has a composition that approximately mimics a bio-oil based on data from Brodin et al. (pyrolyzed Liner Permeate pine/spruce lignin),[38] and the other has approximately equimolar amounts of each monomer to facilitate determination of component-dependent vs composition-dependent property comparisons. The data demonstrate the LBMPs' beneficial T_g's of at least 100 °C (above boiling water but not too high such that processing and energy costs could become problematic), thermal stabilities above 200 °C, and flow resistances that bridge the gap between PS and PMMA (or exceed PMMA in some cases). The relative properties of various LBMPs are examined in the context of their different R-groups. The softwood lignin-based building blocks that constitute the LBMPs are homologous except for the *p*-position moiety, which is either a hydrogen atom or a methyl, ethyl, or formyl group. These minor structural differences measurably influence the polymers' T_g's, thermolysis behavior, and zero-shear viscosities (η_0's), especially in comparisons between the hydrogen substituent and formyl group (T_g and η_0) or ethyl group (thermolysis behavior). Altogether, this work describes the structural heat-flow stability and polymer processability of guaiacylic methacrylate polymers and provides insight into the component-based versus composition-based structure−property relationships that could facilitate future efforts in macromolecular design.

Scheme 1. Color-Coded Nomenclature Utilized Herein and the Scheme for Synthesizing Softwood Lignin-Based Methacrylate Monomers and the Corresponding Polymers[a]

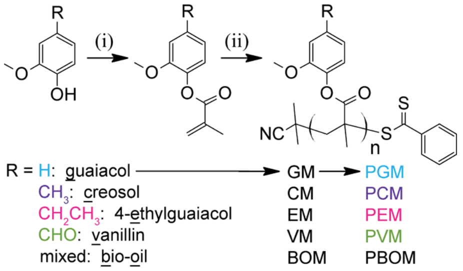

[a] Reagents and conditions: (i) methacrylic anhydride, catalytic 4-(dimethylamino)pyridine, 55 °C, ≥24 h; (ii) 2-cyano-2-propyl benzodithioate, 2,2′-azobis(isobutyronitrile), solvent (see Table S1 for details), 72 °C, ≤10 h.

■ EXPERIMENTAL SECTION

Materials. All lignin-based monomers and polymers were synthesized via acylation and RAFT chemistries, respectively, as depicted in Scheme 1, described in detail elsewhere,[18,23,24,29] and overviewed in Table S1 of the Supporting Information with the macromolecular characteristics (dispersities, molecular weights, etc.) of each LBMP. The monomers are guaiacyl methacrylate (GM) from guaiacol, creosyl methacrylate (CM) from creosol, 4-ethylguaiacyl methacrylate (EM) from 4-ethylguaiacol, and vanillin methacrylate (VM) from vanillin, all of which were prepared by reaction of the phenol with methacrylic anhydride using a catalytic amount of base [4-(dimethylamino)pyridine]. The corresponding polymers are referred to as PGM, PCM, PEM, and PVM, respectively. Hyphenated numbers are used to distinguish between the different materials, in which the value corresponds to the polymer's weight-average molecular weight. Heteropolymers composed of mixtures of these monomers are referred to as poly(bio-oil methacrylate)s or PBOMs.

Nuclear Magnetic Resonance (NMR) Spectroscopy. Compositions of the heteropolymers are listed in Table 1 and were determined using ^{1}H NMR spectroscopy (Bruker AVIII 600 MHz spectrometer, 26 °C, CDCl$_3$ with 0.03 vol % TMS) and characteristic peaks indicated in the literature.[23] The compositions of the heteropolymers do not deviate significantly from the compositions of the monomer mixtures from which the polymers were synthesized at all conversions, as reported previously[23] while confirming the approximately random distribution of monomer segments in each polymer chain.

Table 1. Composition of the PBOMs (in wt %)

monomer	PBOM-22	PBOM-54
EM	28	27
GM	40	25
CM	10	23
VM	22	25

Tacticity of the homopolymers was measured using ^{1}H NMR spectroscopy but with 3 vol % trifluoroacetic anhydride added to the solvent to consume any water in the $CDCl_3$ that can obscure α-methyl protons. Three peaks were fit to each polymers' α-methyl protons using MestReNova NMR software[39] to determine the relative amounts of meso−meso (*mm*) isotactic, meso−racemo (*mr* or *rm*) heterotactic, and racemo−racemo (*rr*) syndiotactic triads, in which the *mm* peak was assumed to be downfield and the *rr* peak was assumed to be upfield of the middle *mr* peak. This assumption follows the peak order and approximate spreading of α-methyl protons reported for PMMA[40] and poly(phenyl methacrylate).[37] The fraction of racemo diads was estimated by normalizing each *mm*, *mr*, and *rr* peak to the total area of all three peaks and then adding *rr* to 0.5 *mr*. The fraction of syndiotactic triads was determined as $rr/(rr + mr + rm + mm)$, in which $mr + rm$ was obtained from a single peak. Select samples also were studied at an elevated temperature (58 °C) with a Bruker AVIII 400 MHz spectrometer to confirm the peak locations of the triads.

Size-Exclusion Chromatography (SEC) with Light Scattering. Molecular weight (number-average, M_n, and weight-average, M_w) and dispersity ($Đ$) data for the polymers were obtained by performing size-exclusion chromatography (SEC) experiments in tetrahydrofuran (THF, 1.0 mL/min) using a Viscotek VE 2001 instrument equipped with a Waters Styragel HR1 and HR4 column (7.8 × 300 mm) in series. A Viscotek multidetector system connected to the SEC instrument consisted of a refractive index (RI) detector (VE3580), an ultraviolet photodiode array (UV-PDA detector), and a viscometer-plus-light-scattering dual detector (270 dual detector), all of which were calibrated with a solution of PS in THF (c = 1.03 mg/mL, M_w = 98 400 g/mol, dn/dc = 0.185 mL/g) immediately prior to data acquisition. Polymer solutions used to evaluate the differential refractive index (dn/dc) and molecular weight for each polymer (Table S1) were prepared at four concentrations (1.0, 0.9, 0.6, and 0.4 mg/mL polymer/THF). RI detector data were used to calculate dn/dc, and light scattering data from scattering angles of 90° and 7° were used to determine absolute molecular weights ($M_{n,LS}$ and $M_{w,LS}$) via Zimm analysis. Hyphenated numbers following a polymer designation correspond to that polymer's $M_{w,LS}$ (kg/mol). Example SEC data for these polymers are shown in Figure S1.

Differential Scattering Calorimetry (DSC). T_g's for each of the LBMPs (PVMs, PCMs, PGMs, PEMs, and PBOMs) were determined using a differential scanning calorimeter (Discovery Series, TA Instruments) with a cell constant and temperature profile calibrated to an indium standard. Polymer powder (2−13 mg), dried at 40 °C under reduced pressure for 48 h, was loaded quantitatively into at least two 20 μL aluminum pans and hermetically sealed in air. Data were collected at 5 °C/min under continuous N_2 flow (50 mL/min) using temperature programs that looped between 0 and 170 °C or 40 and 180 °C, for three heating and cooling cycles. The midpoint of the inflection in the second and third heating traces is reported as the T_g, noting that there were no significant changes between the second and third heating. Error in the T_g measurement is reported at 95% confidence based on DSC data collected using the above temperature programs. The Flory−Fox equation[41]

$$T_g = T_{g\infty} - \frac{K}{M_n} \qquad (1)$$

in which $T_{g\infty}$ is the glass transition temperature expected at infinite molecular weight and K is the empirical Flory−Fox coefficient, was fit to linearized T_g data to approximate the dependence of T_g on M_n. Two outliers (PVM-50, T_g = 118 ± 2 °C and PEM-19, T_g = 92 ± 1 °C) were omitted from the Flory−Fox analysis due to degradation of PVM-50 (see the Supporting Information for more details) and the statistically different tacticity of PEM-19 at 95% confidence (see Table S1).

Thermogravimetric Analysis (TGA). Thermal degradation data for each polymer were collected using a thermogravimetric analyzer (Discovery Series, TA Instruments). Polymer powder (≈5 mg) was loaded quantitatively into 100 μL platinum pans and heated under continuous airflow (10 mL/min sample purge, 5 mL/min balance purge). Samples first were heated at 20 °C/min to 100 °C and annealed for 10−20 min to remove possible water, then were cooled at 10 °C/min to 50 °C and annealed for 1 min, and finally were heated at 10 °C/min to 600 °C for analysis. Percent mass-loss thermolysis profiles were normalized to the mass measured at 100 °C during the final heat. The final mass always matched the empty pan mass within error. Ramp data under continuous N_2 flow (50 mL/min purge for both the balance and sample) and isothermal data under airflow (200 °C for 1 h) also were collected for reference (see Figures S2 and S3).

The characteristic degradation temperatures reported herein are the onset degradation temperature (T_o, the temperature at the intersection of tangents to the initial and steepest segments of the mass-loss data) and the peak degradation temperature (T_p, the temperature at the maximum of the derivative). These characteristic degradation temperatures were chosen because they are not affected by end-group thermolysis and therefore depend minimally on molecular weight.[42] Derivatives of the mass-loss data in the figures are smoothed over 200 data points (100 s of run time) for visual clarity.

Dynamic Mechanical Analysis (DMA). DMA data were collected using an ARES-G2 shear rheometer fitted with 8 mm diameter parallel plates. The polymers for these experiments (PVM-35, PCM-48, PGM-44, PEM-48, PBOM-54, PMMA-55, PS-31, and PS-47) were selected for their similar molecular weights, noting also that PMMA-55 has a similar tacticity to the LBMPs. Polymer discs (0.3 mm in thickness and 8 mm in diameter) were molded at high temperature (170 °C for the LBMPs and PMMA and 150 °C for the PSs) and pressure (1 metric ton per 50 mm^2 sample) for 15 min. The samples were optically clear, and the RAFT-generated LBMPs retained their pink color from the labile benzodithioate end groups (see Figure S4), indicating that end-group thermolysis was not significant during sample preparation.

Frequency sweeps for the LBMPs were acquired at 150, 160, 170, and 180 °C with strain amplitudes between 0.1% and 3.0% in the linear region. The resulting data were shifted by a factor, a_T, to a reference temperature of 150 °C using time−temperature superposition. Frequency sweeps for PS samples, which were analyzed for comparison, were collected at 120, 130, 140, and 150 °C with strain amplitudes ranging from 0.5% to 5.0%, and frequency sweeps for PMMA were collected at 150, 160, 170, 180, 190, and 200 °C with strain amplitudes ranging from 0.4% to 5.0%. These PS and PMMA data also were shifted to a reference temperature of 150 °C. Temperature-dependent data obtained during dynamic shear were obtained at a constant frequency of 6.28 rad/s and strain amplitudes between 0.03% and 5.0%. The temperature range was 100−180 °C for all of the polymers, except for PEM-48 (90−180 °C) and the PSs (90−150 °C) due to the lower PEM and PS T_g's and for PMMA-55 (120−200 °C) due to slippage between the parallel plates at lower temperatures. The maximum temperature for the PS data acquisition was 150 °C because the polymer flowed from between the plates at higher temperatures. The Cox−Merz rule[43] was used to estimate η_0 at the reference temperature (T_{ref}) from the rheology data (see Figure S5), and the dependences of these η_0's on temperature T were estimated from the shift factors [$\eta_0(T) \approx a_T(T)\eta_0(T_{ref})$].

■ RESULTS

Glass Transition Characteristics. The collective T_g's of the homopolymers rank from highest to lowest as PVM, PCM, PGM, and PEM, as illustrated by the $T_{g,\infty}$'s listed in Table 2 and the locations of the endothermic transitions in the example DSC data (normalized to a slope of zero at T = 140−160 °C) shown in Figure 1a. The T_g's for the PBOMs ($T_{g,PBOM\text{-}22}$ = 111 ± 1 °C, $T_{g,PBOM\text{-}54}$ = 119 ± 1 °C) are intermediate to the T_g's of PCM and PGM, as evident by the corresponding molecular-weight-dependent data points in Figure 1b (molecular weight information for all of the polymers is available in the Supporting Information). The Flory−Fox constants from the linear fits to the data in Figure 1b are listed in Table 2 and show that the molecular weight dependence of T_g (K, Table 2) is identical at 95% confidence for all homopolymers, except

Table 2. Properties of Lignin-Based Methacrylate Homopolymers as Determined via Flory−Fox Analysis, DSC, and TGA[a]

parameter	PEM	PGM	PCM	PVM
$T_{g\infty}$ (°C)	116 ± 1	120 ± 3	132 ± 4	139 ± 2
K (g K mol^{-1}) × 10^{-5}	2.0 ± 0.3	2.1 ± 0.9	2.7 ± 0.9	3.6 ± 0.6
dΔH/dT[b] (mW g^{-1} K^{-1})	0.217	0.239	0.216	0.291
T_o (°C)	255 ± 6	302 ± 4	273 ± 3	264 ± 10
T_p (°C)	281 ± 5	327 ± 6	291 ± 5	294 ± 3

[a]Error reported at 95% confidence. [b]Error is ±0.005 mW g^{-1} K^{-1}.

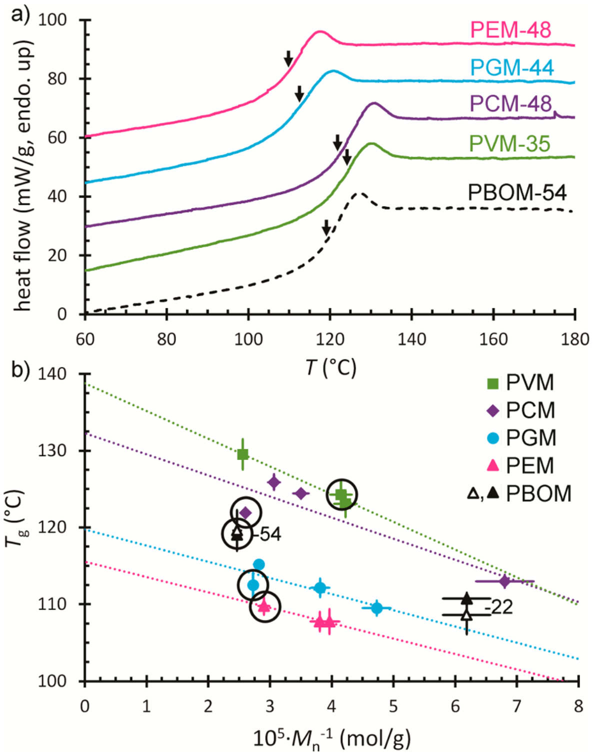

Figure 1. (a) Example DSC data (5 °C/min) and (b) polymer T_g's used in Flory−Fox analysis plotted vs inverse M_n. Data from (a) are mapped onto (b) at the circled positions. The data in (a) (from the polymers also studied by DMA) are shifted vertically, normalized by the slope between 140 and 160 °C, and overlaid with arrows indicating measured T_g's. The data in (b) include error bars that represent 95% confidence in the measurement and color-matched dashed lines that are the linear Flory−Fox fits to the data. The black-filled and black-outlined triangles for the PBOMs represent experimental and predicted (see eq 2) T_g's, respectively. The experimental and predicted T_g's for PBOM-54 (119 ± 1 and 120 ± 3 °C, respectively) are nearly identical aside from the greater error for the predicted value.

between PVM and PEM. Additionally, changes in heat flow with respect to temperature (dΔH/dT) for the homopolymers at T = 60−80 °C are reported in Table 2 (dΔH/dT is 0.218 ± 0.005 mW g^{-1} K^{-1} for PBOM-54). These slopes indicate the relative flexibility of the methacrylate esters,[44] in which PVM and PGM have more rigid ester groups than PCM and PEM. Altogether, these DSC data suggest that a relationship exists between homopolymer R-group, T_g, and dΔH/dT and also between heteropolymer composition and T_g, as discussed in further detail below.

Thermal Degradation Characteristics. On the basis of T_o and T_p listed in Table 2 for the homopolymers, PEM is least stable, PGM is most stable, and PCM and PVM have intermediate stabilities in air. These relative thermal stabilities are illustrated by example data in Figure 2a, in which the onsets and peaks in the PGM data occur at higher temperatures than in the PEM data, and corroborated by data in the Supporting Information (TGA data collected under N_2 flow in Figure S2 and isothermal data taken at 200 °C under airflow in Figure S3). Additionally, the multiple peaks and high-temperature tails in the derivative data for PEM and PVM (and the asymmetry in the data for PCM) indicate that these homopolymers have more complicated degradation pathways in comparison to PGM, which has a single nearly symmetric peak and no measurable tail in the derivative data. Thus, all of these differences in the homopolymer TGA data are attributed to the various R-groups.

For the heteropolymers, PBOM-22 and PBOM-54 have approximately equal thermal stabilities, with T_o's of 257 and 254 °C and T_p's of 277 °C (first peak), 327 °C (second peak) and 278 °C (first peak), 334 °C (second peak), respectively. Two values are reported for T_p in each PBOM example because two distinct peaks exist in the derivatives of the thermolysis profiles, as shown in Figure 2b. The degradation onsets for the PBOMs match the degradation onset of PEM (the corresponding curves in Figure 2a nearly overlap at lower temperatures). Additionally, the peaks for the PBOM data are shifted to slightly lower temperatures relative to the PEM data and slightly higher temperatures relative to the PVM data (see the derivative data in Figure 2a).

PBOM-22 and PBOM-54 have different volatilization rates of the degradation products, which is indicated most clearly by the different peak heights in the derivative data (Figure 2b). These various characteristics of the TGA data likely depend on the PBOM constituents' R-groups as well as the relative compositions of each of the constituents. Finally, all of the LBMPs, homopolymers and heteropolymers alike, have characteristic degradation temperatures that are significantly higher than their T_g's and provide adequate melt processability to ~200 °C.

Viscoelastic Characteristics. DMA data for five LBMPs (PEM-48, PGM-44, PCM-48, PVM-35, and PBOM-54), two PSs (PS-31 and PS-47), and a PMMA (PMMA-55) are presented in Figure 3. Time−temperature superposition master curves of elastic shear moduli (G') vs shifted frequency ($a_T \cdot \omega$) are shown in Figure 3a, and corresponding loss shear moduli (G'') master curves are in the Supporting Information. The overlaid dashed lines in these figures have slopes that approach two (elastic) and one (loss) at low frequencies. These slopes are typical for linear polymers with no significant intermolecular interactions or phase separation in the melt state.[45] G' vs T data are shown in Figure 3b, and complex viscosity (η^*) vs $a_T \cdot \omega$ data are shown in Figure 3c. The slopes of the data in Figures 3b and 3c at melt temperatures ($T > T_g$) and melt frequencies (low $a_T \cdot \omega$), respectively, are reasonably consistent between the LBMPs at each shifted temperature (shifted relative to T_g), indicating that the LBMPs' rheological properties are influenced by temperature and shear in a similar manner. Dissipation factor ($\tan \delta = G''/G'$) vs T data are shown in Figure 3d, and the maxima in these data occur at the rheological T_g's. The vertical and horizontal shifts between the data are mainly due to these different T_α's. Specifically, values for G' and η^* in the melt (at high temperatures or low ω's) in Figures 3a−3c are lowest for the homopolymers with the lowest T_g's and increase in order from PS-31 and PS-47 to

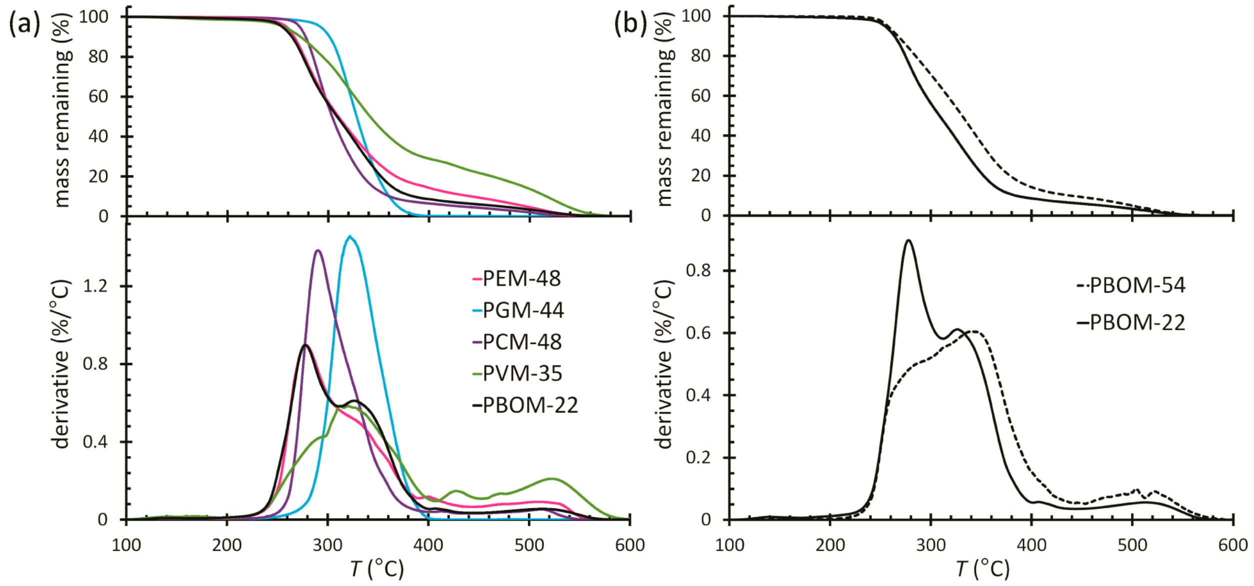

Figure 2. Representative TGA data (10 °C/min, air) for selected LBMPs, in which mass loss (top) and the corresponding derivative (bottom) was obtained on heating. (a) Homopolymers and one PBOM for comparison. (b) Both PBOMs for comparison.

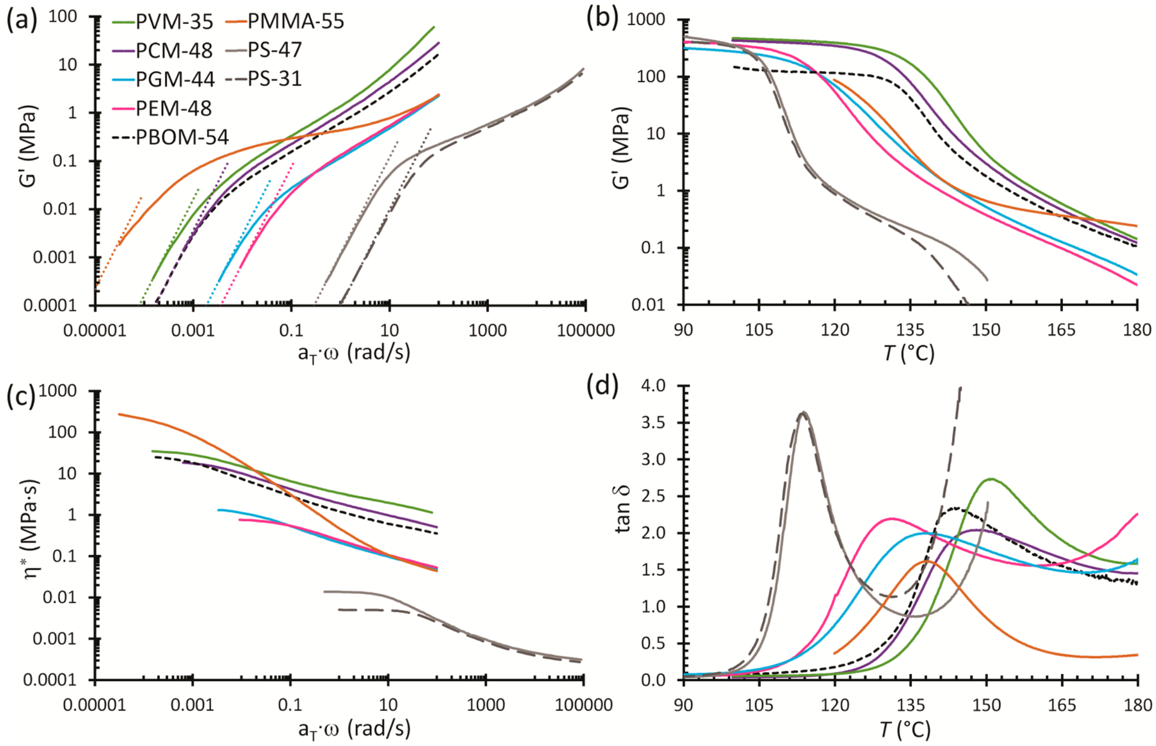

Figure 3. Rheological data for selected LBMPs, two PSs, and a PMMA for comparison. The color-coded legend for all plots is shown in panel (a). (a) The elastic shear modulus (G') for each polymer plotted as a function of frequency (ω) and shifted by factor a_T to a reference temperature of 150 °C using time−temperature superposition. The linear dotted lines have slopes of two to illustrate the expected behavior at low frequencies for polymers with minimal intermolecular interactions. (b) Temperature-dependent G' for each polymer measured at a constant ω of 6.28 rad/s, ramp rate of 3 °C/min, and strain amplitude between 0.03% and 5.0%. (c) Complex viscosity (η^*) for each polymer plotted as a function of $a_T \cdot \omega$ as described in (a). The corresponding dynamic viscosity (η) vs shear rate plot for determining zero-shear viscosities (η_0's, Table 3) is in the Supporting Information. (d) Temperature-dependent dissipation factor (tan δ) for each polymer determined using the conditions and data reported for (b) and the corresponding loss moduli reported in the Supporting Information. The location of the maximum in each tan δ trace was taken as T_α, the rheological T_g.

PEM-48, PGM-44, PCM-48, and PVM-35 to PMMA-55. Values for G' and η^* for PBOM-54 are mostly located between the corresponding values for PGM-44 and PCM-48 (Figures 3a−3c), as expected based on PBOM-54's intermediate T_α to PGM-44 and PCM-48; however, at the lowest $a_T \cdot \omega$'s in Figures 3a and 3c, the values for PBOM-54 begin to exceed those for PCM-48 and approach those for PVM-35. This crossover may indicate that VM segments in PBOM-54 disproportionality influence the viscoelasticity of the heteropolymer in the melt, as discussed in further detail below. Overall, the temperature- and time-dependent changes in viscoelasticity shown in Figure 3 are mostly independent of R-group, aside from the horizontal and vertical shifts.

In contrast, the R-group plays a vital role in the η_0's listed in Table 3 and shown in Figure 4. The LBMP T_α's span 19 °C, and the LBMP η_0's (at 150 °C) span nearly 2 orders of magnitude. In both cases, PVM-35 and PCM-48 have the highest values and PEM-48 has the lowest. This ordering is consistent with the ordering based on $T_{g\infty}$'s (Table 2). Additionally, at 150 °C, the η_0 for PEM-48 is nearly 2 orders of magnitude larger than the η_0 for PS-47 yet less than the η_0 for atactic PMMA-55 and other similar PMMAs from the literature.[46] These viscosity data indicate that the LBMPs may be less prone to deformation under normal use conditions, with respect to time, temperature, or shear, in comparison to PS, while maintaining the processability of PMMA.

Table 3. Properties of Selected Polymers as Determined Using SEC (Light Scattering) and DMA[a]

polymer	$M_{w,LS}$ (g/mol)	Đ	T_α (°C)	η_0[b] (kPa s)
PEM-48	48 000	1.39	132	730
PGM-44	44 000	1.20	138	1300
PCM-48	48 000	1.26	148	18 000
PVM-35	35 000	1.47	151	34 000
PBOM-54	54 000	1.33	144	25 000
PMMA-55	55 000	1.54	138	270 000
PS-31	31 000	1.23	114	5.0
PS-47	47 000	1.18	114	14

[a] Thermal and macromolecular property data for these polymers are shown in Figures 1−4. A full list of polymers, synthesis conditions, and characteristics is available in the Supporting Information. [b] T_{ref} = 150 °C.

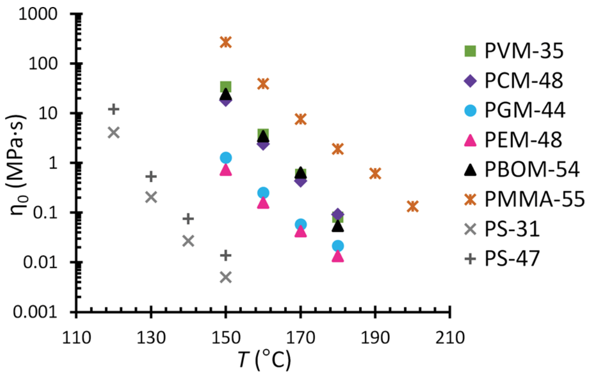

Figure 4. Zero-shear viscosity vs. temperature data determined by normalizing the shift factors that were used to construct master curves (Figures 3a and 3c, Figure S6a) with the η_0's at T_{ref} = 150 °C.

Finally, PBOM-54's T_α is consistent with its DSC-based T_g, which is between the T_g's for PGM and PCM, as listed in Table 3 and shown by the relative shifts of the data in Figure 3d; however, PBOM-54's η_0 is intermediate to the η_0's for PCM-48 and PVM-35. This difference indicates that there may be a disproportionate dependence between VM content and heteropolymer properties, as mentioned above in reference to Figures 3a and 3c.

■ DISCUSSION

The lignin-based monomers and polymers described herein are significant for at least four main reasons. First, these LBMPs are considered "green" for the constituents' low volatility and low toxicity according to estimates made via the Environmental Protection Agency's Estimation Program Interface Suite (EPI Suite)[47] and for their potentially high bio-based contents (64−69%, or 100% assuming the methacrylate group comes from renewable resources in the future).[18,24] Second, as indicated in the above results, the bio-based monomers yield materials with beneficial properties in comparison to PS, with respect to their reduced tendency for deformation, and PMMA, with respect to processability. Third, the structural differences between polymers provide insight into structure−property relationships that are increasingly relevant as more homologous monomers are extracted from biomass or prepared using biological means. Finally, the heteropolymers are expected to provide a means for reducing costs and tuning properties, which herein involves choosing η_0's without compromising the promising T_g's, thermal stabilities, and other viscoelastic properties.

Homopolymer Structure−Property Relationships. *Glass Transition Temperatures.* The most important detail regarding the T_g-practicality of the softwood LBMPs is that they have T_g's near and above that of boiling water, but the T_g's are not so high that processing and energy costs could become problematic. Two polymers have T_g's that are a close match to the 100 °C T_g of PS (PEM-19 and PEM-30 have T_g's of 92 ± 1 and 108 ± 2 °C, respectively), while another polymer has a T_g as high as 130 ± 2 °C (PVM-53). The proximity of some of these LBMP T_g's to 100 °C is among the closest reported to date for bio-based thermoplastics from linear and narrow-dispersity macromolecules.[1,19,20,22]

Differences between the T_g's for the LBMPs are direct consequences of their different R-groups and molecular weights, not of tacticity variations. This assertion was supported by measuring the fractions of racemo diads $[r/(r + m)]$ and syndiotactic triads $[rr/(rr + rm + mr + mm)]$ via the α-methyl protons in ^{1}H NMR spectroscopy data. Example spectra are shown in Figure 5. The average racemo diad percentages were 79 ± 3% for the PVMs, 78 ± 2% for the PCMs, 71 ± 1% for

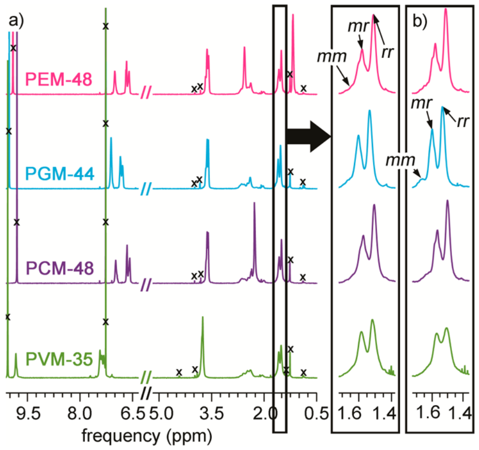

Figure 5. Example ^{1}H NMR spectra obtained at (a) 26 °C, 600 MHz and (b) 58 °C, 400 MHz for the softwood LBMPs that were studied using DMA. α-Methyl peaks utilized to quantify tacticity are shown in the expanded region. Peaks marked with x's in the full spectra (trifluoroacetic acid, chloroform, etc.) are solvent peaks.

the PGMs, and 73 ± 8% for the PEMs. These values are consistent with atactic methacrylate polymers, which have racemo diad percentages of approximately 70%.[32] The syndiotactic triad percentages (see the Supporting Information) were somewhat more variable, yet still consistent between polymers, and also suggestive of atactic polymers.

To draw relevant comparisons between the R-groups and T_g's that could inform future QSPR models and molecular designs, molecular weight effects also were eliminated by fitting the T_g data with the Flory−Fox equation (eq 1, Table 2). In order of increasing $T_{g\infty}$, the polymers rank as PEM, PGM, PCM, and PVM and exhibit T_g's that span ≈20 °C at similar molecular weights. This ordering is consistent with Saito et al.'s finding that greater aliphatic and guaiacylic carbon content in oligomeric softwood lignins corresponds to lower T_g's.[31] This small T_g-gap indicates that although R-group influences T_g, its significance is minor in comparison to expected tacticity effects.[32,33,35]

The relative T_g's between the LBMPs can be explained in part by applying qualitative free volume and rigidity principles. Molecular movements thought to contribute most to the relative T_g's of the LBM homopolymers are depicted in Figure 6. Flexible R-groups should increase free volume and consequently lower T_g;[48] this relationship is consistent for PEM's T_g in comparison to PGM's T_g. The ethyl moiety can bend along at the R-group's CH_3-CH_2 bond and rotate around the CH_2−phenol bond to open up free space, whereas the hydrogen atom (and the methyl and formyl groups) lacks these degrees of freedom for movement. In contrast, rigid R-groups should reduce free volume by sterically hindering side-chain motion and consequently raise T_g; this relationship also is consistent for PCM's and PVM's T_g's in comparison to PGM's T_g. In these examples, the bulky, yet stiff, methyl (PCM) and aldehyde (PVM) groups restrict rotation of the phenolic group around the phenol−ester linkage, decreasing backbone flexibility.

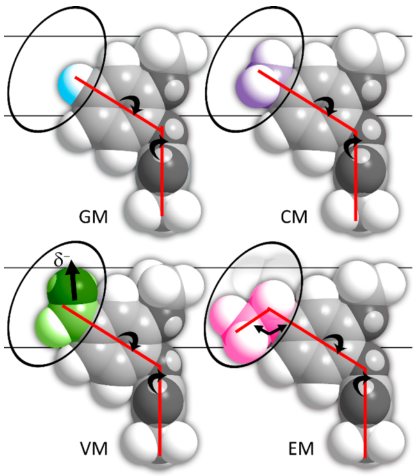

Figure 6. Space-filling models to illustrate the differences between monomer R-groups, which are highlighted in color and by black ellipses. Red lines signify important axes of rotation or bending, black lines and ellipses are visual cues to R-group size, single-headed curved arrows represent rotational movement, the double-headed bent arrow indicates flexural movement, and the single-headed straight arrow denotes polarity. The aromatic rings and methacrylate esters are oriented approximately parallel and perpendicular to the page, respectively.

Additionally, PVM's higher T_g in comparison to PCM results from the reduced mobility of the methacrylate ester. Evidence for differences in ester group mobility are available in the DSC and ^{1}H NMR spectroscopy data (Figures 1a and 5, respectively) for the LBM homopolymers. First, the slope of the DSC data for the LBMPs at $T \ll T_g$ ($d\Delta H/dT$, Table 2 and Figure 1a) is steepest for PVM, suggesting that it has less ester-group mobility than the other LBMPs.[44] Second, the peaks shown in Figure 5 that represent backbone α-methyl protons are broader and less well-defined for PVM than for the other LBMPs. This qualitative difference is a possible indication that the PVM backbone is not as flexible as that of the other polymers, which may result from polarity differences between the various homopolymers. Specifically, polymer polarity should decrease from PVM to PGM to PCM/PEM, the same order of decreasing slopes in the DSC data. This ranking of polarities is consistent based on the electron-donating/electron-withdrawing character of the R-groups;[49] ^{1}H NMR data,[23] in which the chemical shifts of the vinyl protons are furthest downfield for the most polar monomers due to the electron-withdrawing character (polarity) of the ester group; and hydrophobicity predictions made using Mathers et al.'s method[50] with ACD/Laboratories,[51] EPI Suite,[47] and Chem-Bio3D[52] software. Together, these data support that PVM, the likely most polar macromolecule, has the most rigid methacrylate ester group and thus a higher T_g relative to the other LBMPs.

Overall, these thermal transition data clearly indicate that these modest adjustments to the *p*-position R-groups measurably influence T_g's. Other R-groups, from bio-based or synthetic materials, may affect aromatic polymer T_g's in similar ways, so the reported structure−T_g relationships herein can provide guidance for future macromolecular designs.

Thermal Degradation Temperatures. The characteristic thermal degradation temperatures for the LBMPs (Table 2) are at least 100 °C greater than the T_g's (Figure 1), indicating that these polymers all should be amenable to melt processing and thermoforming in air unless temperatures greater than 250 °C are required. As with T_g, the relative thermal degradation characteristics of the LBMPs (Figure 2a) result from differences in R-groups. PEM is least stable, PGM is most stable, and PCM and PVM have intermediate stabilities. PEM degrades at the lowest temperature likely because the CH_2-CH_3 bond is the weakest bond in any of the R-groups; the lowest R-group-associated bond dissociation energy is 301 kJ/mol for a $C_6H_5\mathbf{CH_2}-\mathbf{CH_3}$ (EM) bond, 356 kJ/mol for a $C_6H_5\mathbf{CH_2}-\mathbf{H}$ (CM) bond, 364 kJ/mol for a $C_6H_5\mathbf{C}(=\mathbf{O})-\mathbf{H}$ (VM) bond, and 473 kJ/mol for a $\mathbf{C_6H_5}-\mathbf{H}$ (GM) bond.[49,53] Conversely, PGM is the most thermally stable of the softwood LBMPs and likely degrades by random scission of the polymer backbone due to the R-group's high bond dissociation energy. This hypothesis is supported in that PGM's peak degradation temperature of ∼330 °C (10 °C/min under flowed air; between 370 and 380 °C at 10 °C/min under flowed N_2, as shown in Figure S2) is independent of M_w and similar to that of RAFT-generated PMMA's higher peak degradation temperature of ∼360−380 °C (5 °C/min under N_2) that is thought to correspond to a chain-scission mechanism.[54] Additionally, the unimodal peak in the derivative of the TGA data for PGM suggests that only a single polymer thermolysis process is significant in air. The N_2-based thermolysis data in Figure S2 are more complicated due to the elimination of oxygen that can consume radicals as they are generated and hence the greater possibility for unzipping from the end groups.[54] In both the air and N_2 TGA data, the comparably complicated and multimodal thermolysis profile for PVM likely is a direct consequence of the formyl group. Aldehydes are inherently reactive, so the complexity of the thermolysis data could arise from multiple reaction types being involved in the breakdown of the polymer. Some of the reactions likely result in the formation of temporary char, the source of the significant tail in the TGA data for PVM at $T > 400$ °C (Figure 2a).[55] Overall, these TGA data indicate that the most stable of the studied softwood LBMPs has a hydrogen atom as an R-group, the least stable has an *n*-alkyl R-group, and the most char-forming has a formyl R-group.

Viscoelasticity. The LBMPs have increased η_0's and otherwise consistent temperature- and frequency-dependent viscoelastic performance relative to PS, but the η_0's and rheological properties deviate from those of PMMA-55 by significantly differing amounts. These characteristics indicate that the LBMPs may be less prone to deformation from natural temperature- and time-dependent flow processes in comparison to PS, but LBMP deformation in comparison to PMMA depends largely on R-group, discussed more in later paragraphs. In general, the LBMPs are less or similarly viscous as PMMA-55 (even after normalization by $M_{w,LS}$ and considering that the higher $Đ$ of PMMA-55 lowers its η_0 in comparison to the other polymers) and other PMMAs from literature,[46] so they could be preferable for certain applications. Mainly, these viscosities that are intermediate to those of PS and PMMA may provide a means for balancing trade-offs between materials longevity and processability for various applications in adhesives, thermoplastic elastomers, or building and vehicle components.

Although the LBMPs have generally attractive η_0's, the entanglement molecular weight (M_e) for the LBMPs may be somewhat less desirable. Evidence for the different M_e's between PS, PMMA, and the LBMPs is found mainly in the G' data (Figure 3b). Specifically, the PS traces in Figure 3b have sharper inflections and shallower slopes (features of a plateau modulus that start to become apparent at $M_w > 2M_e$) than the LBMP traces of similar M_w polymers, and these features are even more pronounced for PMMA-55. A significant difference in M_e is expected because M_e generally increases with increasing side-chain bulkiness; atactic PS and atactic poly(4-*t*-butylstyrene) have M_e's of 17 000 and 38 000 g/mol, respectively,[56] while atactic poly(methyl methacrylate) has an M_e near 7000 g/mol.[46]

No definitive relationships exist between the studied LBMP R-groups and the shear moduli (or differential changes to the shear moduli) with respect to temperature or frequency, as shown in the rheology data (Figure 3a,b,d and Figure S6). Both the magnitudes and slopes of the shear moduli data for the melt are similar relative to T_α given the slight variations in molecular weight and dispersity, as was described in the Results section. These similarities were expected given that the LBMPs likely have similar M_e's.

Unlike the modulus data, the η_0's significantly depend on R-group, spanning nearly 2 orders of magnitude between PEM-48 and PVM-35. The ranking of polymers based on η_0's is consistent with their ranking based on T_g, so the qualitative free volume and polarity arguments mentioned above (e.g., Figure 6) likely apply here as well. Interestingly, the large differences between η_0's compared to the ≈20 °C differences between T_g's suggest that viscosity may be more sensitive to R-group than T_g. For example, the rigid methyl and aldehyde groups may prevent polymer chains from sliding past each other, either through possible physical or (for PVM) dipole−dipole interactions. Regardless, a number of quantitative yet semi-empirical models[57,58] support that T_g and η_0 are interrelated, consistent with the assertion herein that both T_g and η_0 are measurably dependent on R-group for reasons of rigidity, free volume, and possibly polarity.

Overall, the LBMPs have mostly intermediate flow characteristics in comparisons to PSs and PMMAs of similar molecular weights, making the LBMPs excellent candidates as glassy blocks, but to differing degrees, as the η_0's span almost 2 orders of magnitude. The elastic and loss shear moduli are significantly less R-group-dependent than η_0, allowing one to choose a desired η_0 without significantly changing other mechanical shear properties. Hence, functionalized components of softwood lignin bio-oils provide a convenient platform for accessing a range of thermal and viscoelastic polymer properties without compromising other beneficial material characteristics.

Heteropolymer Composition−Property Relationships. *Glass Transition Temperatures.* The T_g for a heteropolymer can be predicted by utilizing compositional information. Various forms of the Fox equation empirically relate the weight fraction of each monomer type within a heteropolymer to the T_g of the heteropolymer. In this work, the following form was used:

$$\frac{1}{T_{g,PBOM}} = \sum \frac{w_i}{T_{g,i}} \tag{2}$$

in which $T_{g,PBOM}$ (K) is the T_g of the heteropolymer, $T_{g,i}$ (K) is the T_g for a homopolymer composed of monomer i estimated via eq 1 and the Flory−Fox constants from Table 2, and w_i is the weight fraction of monomer i in the heteropolymer (Table 1). This method yields predicted T_g's for PBOM-22 and PBOM-54 of 109 ± 3 and 120 ± 3 °C, respectively, which match the measured T_g's of 111 ± 1 and 119 ± 1 °C, respectively. The agreement between the measured and predicted T_g's supports the assertion that the tacticities of the homopolymers and heteropolymers are similar. These features of predictability and consistent tacticity are invaluable if precise T_g's are important for a particular application.

Thermal Degradation Temperatures. Heteropolymers likely are as stable as the least stable component, as suggested by comparing the consistent T_o's of 254−257 °C for PBOM-22, PBOM-54, and the PEMs, which all contain segments with ethyl R-groups. Consequently, some level of bio-oil fractionation may be necessary if a heteropolymer for a given application requires a higher thermal stability than $T_g + 100$ °C.

The degradation rates (the derivative TGA data [Figure 2], which herein are the release rates of volatiles) of the heteropolymers likely depend on the composition of the overall chains, not just EM content. PBOM-22 degrades faster than PBOM-54; it has the higher peak degradation rate in the derivative data shown in Figure 2b. Thermolysis can begin at chain ends,[54] so the higher end group concentration in PBOM-22 may be one reason that this heteropolymer degrades faster than PBOM-54; however, composition likely is a significant factor as well. In this example, PBOM-54 (25 wt % VM) contains more VM segments than PBOM-22 (22 wt % VM), and the mass remaining is consistently higher for PBOM-54 than PBOM-22 (by 3−8 wt % units from 260 to 400 °C). As char-formers (e.g., VM as discussed in the corresponding homopolymer section) in polymers can reduce material

DOI: 10.1021/acs.macromol.5b02316
Macromolecules XXXX, XXX, XXX−XXX

flammability by disproportionately reducing volatiles formation and release,[55] these different VM contents may be responsible for (at least partially) the different TGA-based degradation rates. Furthermore, PBOM-22 and PBOM-54 contain similar mass fractions of EM segments (Table 1), and PCM and PGM have nearly the same peak degradation rates (Figure 2a), so EM, CM, and GM components likely are not contributing significantly to the relative degradation rates of the PBOMs. Overall, the thermal stabilities and degradation rates of PBOMs can be tuned by eliminating the least stable components (EM) and adjusting the content of char-formers (VM), as the factors that influence heteropolymer thermolysis are likely both component-based and composition-based.

Viscoelasticity. The viscosity and shear modulus data for PBOM-54 exhibit the same differential changes with respect to temperature and frequency as the LBM homopolymers (Figures 3 and 4, Figures S5 and S6), yet the η_0 is disproportionately dependent on VM content based mainly on η_0 for PBOM-54 being closest to η_0 for PVM. Additionally, averages weighted by M_w (η_0 is proportional to M_w for $M_w < M_e$)[45] and composition consistently underestimated η_0, suggesting that η_0 may be more component-dependent than composition-dependent. The cause for VM's disproportionate effect on η_0 may be its polarity (or possibly dipole−dipole interactions). Overall, these DMA data suggest that viscoelastic properties of heteropolymers likely are more component-dependent than composition-dependent.

■ CONCLUSION

As demonstrated by this library of softwood lignin-based methacrylate monomers, structural differences between the *p*-position R-groups in guaiacylic methacrylates measurably affect the glass transition, thermal degradation, and viscoelastic properties of corresponding polymers. All of the polymers are stable thermally to at least 100 °C above the T_g, suggesting that LBMPs should be amenable to melt processing. PVM and PCM, with formyl and methyl functional groups, respectively, have the most rigid R-groups and consequently the highest T_g's and η_0's in comparison to PGM and PEM. Interestingly, the R-group affects η_0 much more than it affects T_g, T_o, and T_p. Finally, all of the LBMPs, homopolymers and heteropolymer alike, have superb viscoelastic character for improving the shear flow stability of plastics.

The reported composition−property and component−property relationships further inform what separation steps may be necessary to tune *a priori* the properties of heteropolymers prepared from mixtures of softwood lignin bio-oils. The least thermally stable EM segments dictate the degradation onset, and the char-forming VM segments reduce the release rate of volatiles during thermolysis. Furthermore, the VM segments contribute most significantly to PBOM's η_0. Together, and in agreement with the Fox equation, all of the monomers, whether GM, EM, CM, or VM, proportionally contribute to the T_g based on their relative contents.

Importantly, the components of the studied polymers can be prepared from an inexpensive and abundant biomass. The consistent and predictable characteristics between LBMPs and heteropolymers further indicate that separations at a lignin bio-oil refinery may not need to be incredibly stringent for polymers applications, tolerating compositional variations without significantly changing the expected material performance. Hence, the guaiacolic components of softwood lignin-based bio-oils constitute a convenient and potentially inexpensive bio-based platform for the synthesis of practical new materials.

■ ASSOCIATED CONTENT

Supporting Information

The Supporting Information is available free of charge on the ACS Publications website at DOI: 10.1021/acs.macromol.5b02316.

Polymer synthesis conditions and macromolecular characteristics; example SEC data; photograph of DMA samples; and additional TGA and DMA data (PDF)

■ AUTHOR INFORMATION

Corresponding Author

*E-mail: thepps@udel.edu (T.H.E.).

Notes

The authors declare no competing financial interest.
R.P.W.: Deceased 24 March 2015.

■ ACKNOWLEDGMENTS

The authors from the University of Delaware (UD) Department of Chemical and Biomolecular Engineering acknowledge NSF Grant CHE-1507010 and AFOSR-PECASE Grant FA9550-09-1-0706 for partial financial support. The authors from the UD Center for Composite Materials acknowledge a SERDP WP-1758 through the Cooperative Agreement W911NF-06-2-001 for partial financial support. N.A.N. acknowledges the UD Department of Materials Science and Engineering and NIST Award 70NANB10H256 through the UD Center for Neutron Science for financial support. The UD NMR facility used for this project was supported by the Delaware COBRE program with a grant from the National Institute of General Medical Sciences−NIGMS (1 P30 GM110758-01) from the National Institutes of Health. The authors thank Scott R. Horton and Prof. Michael T. Klein for helpful discussions; Prof. Joseph F. Stanzione, III, for providing some monomer; Prof. Michael E. Mackay for use of the rheometer; and the UD Advanced Materials Characterization Lab for use of the DSC and TGA instruments.

■ REFERENCES

(1) Holmberg, A. L.; Reno, K. H.; Wool, R. P.; Epps, T. H., III *Soft Matter* **2014**, *10* (38), 7405−7424.

(2) Tschan, M. J. L.; Brule, E.; Haquette, P.; Thomas, C. M. *Polym. Chem.* **2012**, *3* (4), 836−851.

(3) Mülhaupt, R. *Macromol. Chem. Phys.* **2013**, *214* (2), 159−174.

(4) Fache, M.; Boutevin, B.; Caillol, S. *Green Chem.* **2016**, Advance Article; DOI: 10.1039/c5gc01070e.

(5) Miller, S. A. *ACS Macro Lett.* **2013**, *2* (6), 550−554.

(6) Isikgor, F. H.; Becer, C. R. *Polym. Chem.* **2015**, *6* (25), 4497−4559.

(7) Mathers, R. T. *J. Polym. Sci., Part A: Polym. Chem.* **2012**, *50* (1), 1−15.

(8) Laurichesse, S.; Avérous, L. *Prog. Polym. Sci.* **2014**, *39* (7), 1266−1290.

(9) Fache, M.; Boutevin, B.; Caillol, S. *Eur. Polym. J.* **2015**, *68*, 488−502.

(10) Satoh, K.; Saitoh, S.; Kamigaito, M. *J. Am. Chem. Soc.* **2007**, *129* (31), 9586−9587.

(11) Miyake, G. M.; Newton, S. E.; Mariott, W. R.; Chen, E. Y. X. *Dalton Transactions* **2010**, *39* (29), 6710−6718.

(12) Ding, K.; John, A.; Shin, J.; Lee, Y.; Quinn, T.; Tolman, W. B.; Hillmyer, M. A. *Biomacromolecules* **2015**, *16* (8), 2537−2539.

(13) Gowda, R. R.; Chen, E. Y. X. *Org. Chem. Front.* **2014**, *1* (3), 230−234.

(14) Gustafson, T. P.; Lonnecker, A. T.; Heo, G. S.; Zhang, S.; Dove, A. P.; Wooley, K. L. *Biomacromolecules* **2013**, *14* (9), 3346−3353.

(15) Bolton, J. M.; Hillmyer, M. A.; Hoye, T. R. *ACS Macro Lett.* **2014**, *3* (8), 717−720.

(16) Satoh, K.; Nakahara, A.; Mukunoki, K.; Sugiyama, H.; Saito, H.; Kamigaito, M. *Polym. Chem.* **2014**, *5* (9), 3222−3230.

(17) Satoh, K.; Sugiyama, H.; Kamigaito, M. *Green Chem.* **2006**, *8* (10), 878−882.

(18) Holmberg, A. L.; Stanzione, J. F., III; Wool, R. P.; Epps, T. H., III *ACS Sustainable Chem. Eng.* **2014**, *2* (4), 569−573.

(19) Gallagher, J. J.; Hillmyer, M. A.; Reineke, T. M. *ACS Sustainable Chem. Eng.* **2015**, *3* (4), 662−667.

(20) Satoh, K. *Polym. J.* **2015**, *47* (8), 527−536.

(21) Iwata, T. *Angew. Chem., Int. Ed.* **2015**, *54* (11), 3210−3215.

(22) Yao, K.; Tang, C. *Macromolecules* **2013**, *46* (5), 1689−1712.

(23) Holmberg, A. L.; Karavolias, M. G.; Epps, T. H., III *Polym. Chem.* **2015**, *6* (31), 5728−5739.

(24) Stanzione, J. F., III; Giangiulio, P. A.; Sadler, J. M.; La Scala, J. J.; Wool, R. P. *ACS Sustainable Chem. Eng.* **2013**, *1* (4), 419−426.

(25) Wang, S.; Vajjala Kesava, S.; Gomez, E. D.; Robertson, M. L. *Macromolecules* **2013**, *46* (18), 7202−7212.

(26) Jegers, H. E.; Klein, M. T. *Ind. Eng. Chem. Process Des. Dev.* **1985**, *24* (1), 173−183.

(27) Asmadi, M.; Kawamoto, H.; Saka, S. *J. Anal. Appl. Pyrolysis* **2011**, *92* (2), 417−425.

(28) Choi, H. S.; Meier, D. *J. Anal. Appl. Pyrolysis* **2013**, *100*, 207−212.

(29) Stanzione, J. F., III; Sadler, J. M.; La Scala, J. J.; Wool, R. P. *ChemSusChem* **2012**, *5* (7), 1291−1297.

(30) Yoshida, T.; Lu, R.; Han, S.; Hattori, K.; Katsuta, T.; Takeda, K.-I.; Sugimoto, K.; Funaoka, M. *J. Polym. Sci., Part A: Polym. Chem.* **2009**, *47* (3), 824−832.

(31) Saito, T.; Perkins, J. H.; Vautard, F.; Meyer, H. M.; Messman, J. M.; Tolnai, B.; Naskar, A. K. *ChemSusChem* **2014**, *7* (1), 221−228.

(32) Bertinetto, C.; Duce, C.; Micheli, A.; Solaro, R.; Starita, A.; Tiné, M. R. *Polymer* **2007**, *48* (24), 7121−7129.

(33) Soldera, A.; Metatla, N. *Phys. Rev. E* **2006**, *74* (6), 061803.

(34) Rogers, S.; Mandelkern, L. *J. Phys. Chem.* **1957**, *61* (7), 985−991.

(35) Ute, K.; Miyatake, N.; Hatada, K. *Polymer* **1995**, *36* (7), 1415−1419.

(36) Otsu, T.; Yamada, B.; Sugiyama, S.; Mori, S. *J. Polym. Sci., Polym. Chem. Ed.* **1980**, *18* (7), 2197−2207.

(37) Wesslén, B.; Gunneby, G.; Hellström, G.; Svedling, P. *J. Polym. Sci., Polym. Symp.* **1973**, *42* (1), 457−465.

(38) Brodin, I.; Sjöholm, E.; Gellerstedt, G. *J. Anal. Appl. Pyrolysis* **2010**, *87* (1), 70−77.

(39) MestReNova, version 10.0.2, Mestrelab Research, S.L: Santiago de Compostela, Spain, 2014.

(40) Bovey, F. A.; Tiers, G. V. D. *J. Polym. Sci.* **1960**, *44* (143), 173−182.

(41) Fox, T. G.; Flory, P. J. *J. Appl. Phys.* **1950**, *21* (6), 581−591.

(42) *Frequently Asked Questions: Thermogravimetric Analysis (TGA), A Beginner's Guide*; PerkinElmer: Waltham, MA, 2010; http://www.perkinelmer.com/CMSResources/Images/44-74556GDE_TGABeginnersGuide.pdf (accessed Oct 24, 2013).

(43) Cox, W. P.; Merz, E. H. *J. Polym. Sci.* **1958**, *28* (118), 619−622.

(44) Karasz, F. E.; MacKnight, W. J. *Macromolecules* **1968**, *1* (6), 537−540.

(45) Morrison, F. A. *Understanding Rheology*; Oxford University Press: New York, 2001.

(46) Fuchs, K.; Friedrich, C.; Weese, J. *Macromolecules* **1996**, *29* (18), 5893−5901.

(47) *EPI Suite Version 4.11*, U.S. Environmental Protection Agency, Washington, DC, Nov 2012.

(48) Dudowicz, J.; Freed, K. F.; Douglas, J. F. *J. Phys. Chem. B* **2005**, *109* (45), 21285−21292.

(49) Wade, L. G. *Organic Chemistry*, 6th ed.; Pearson Prentice Hall: Upper Saddle River, NJ, 2006.

(50) Magenau, A. J. D.; Richards, J. A.; Pasquinelli, M. A.; Savin, D. A.; Mathers, R. T. *Macromolecules* **2015**, *48* (19), 7230−7236.

(51) ACD/ChemSketch (Freeware) 2015, version C10E41, Advanced Chemistry Development, Inc.: Toronto, ON, Canada, acdlabs.com, 2015.

(52) ChemBio3D Ultra, version 14.0.0.117, PerkinElmer, Inc., Waltham, MA, 2014.

(53) Dean, J. A.; Lange, N. A. *Lange's Handbook of Chemistry*; McGraw-Hill: New York, 1992.

(54) Chong, B.; Moad, G.; Rizzardo, E.; Skidmore, M.; Thang, S. H. *Aust. J. Chem.* **2006**, *59* (10), 755−762.

(55) Camino, G.; Costa, L. *Polym. Degrad. Stab.* **1988**, *20* (3−4), 271−294.

(56) Fetters, L. J.; Lohse, D. J.; Colby, R. H. Chain Dimensions and Entanglement Spacings. In *Physical Properties of Polymers Handbook*; Mark, J., Ed.; Springer-Verlag: New York, 2007; pp 447−454.

(57) Wool, R. P. *J. Polym. Sci., Part B: Polym. Phys.* **2008**, *46* (24), 2765−2778.

(58) Williams, M. L.; Landel, R. F.; Ferry, J. D. *J. Am. Chem. Soc.* **1955**, *77* (14), 3701−3707.

DOI: 10.1021/acs.macromol.5b02316
Macromolecules XXXX, XXX, XXX−XXX